TRENDS IN SCIENCES 2026; 23(11): 13366
https://doi.org/10.48048/tis.2026.13366 RESEARCH ARTICLE

Astrocytic Changes in the Striatum and Hippocampus in A Rat Model of Human Methamphetamine Abuse

Walailuk Kerdsan-Phusan[1], Samur Thanoi[1], Gavin P. Reynolds[2,4] and Sutisa Nudmamud-Thanoi[3,4,5,*]

[1]School of Medical Sciences, University of Phayao, Phayao 56000, Thailand
[2]Biomolecular Sciences Research Centre, Sheffield Hallam University, Sheffield S1 1WB, United Kingdom
[3]Department of Anatomy, Faculty of Medical Science, Naresuan University, Phitsanulok 65000, Thailand
[4]Centre of Excellence in Medical Biotechnology, Faculty of Medical Science, Naresuan University, Phitsanulok 65000, Thailand
[5]Frontier Research Cluster in Brain Health, Naresuan University, Phitsanulok 65000, Thailand

([*]Corresponding author's e-mail: sutisat@nu.ac.th)

Received: 16 January 2026, Revised: 7 April 2026, Accepted: 14 April 2026, Published: 1 June 2026

Abstract

Methamphetamine (METH) is a highly addictive psychostimulant that exerts profound effects on the central nervous system, including psychosis, cognitive impairment, and memory disturbances. Chronic METH use disrupts neurotransmitter homeostasis and neuronal circuitry, contributing to long-term neurotoxicity. Astrocytes, as key regulators of synaptic transmission and brain homeostasis, are likely involved in METH-induced neuropathology. This study investigated astrocytic responses in specific brain regions, namely the striatum, nucleus accumbens, and hippocampus, using a rodent METH exposure paradigm that mimics human patterns of abuse. Immunohistochemical analysis of glial fibrillary acidic protein (GFAP) was performed in sham control, acute binge, escalating dose, and escalating dose-binge METH groups. Results showed increased GFAP immunoreactivity consistent with reactive astrogliosis, particularly in the escalating dose-binge group, suggesting heightened susceptibility in the striatum and hippocampus. Notably, region-specific astrocytic responses were observed: increased numbers of GFAP-positive cells without corresponding GFAP area expansion in the nucleus accumbens core, nucleus accumbens shell, and hippocampal CA2 subregion, suggesting a relatively mild astrocyte reactivity with limited cytoskeletal remodeling. In contrast, increased GFAP area without a corresponding increase in the number of GFAP-positive cells in the dorsolateral subregion of the striatum suggested features consistent with astrocytic hypertrophy or process elongation. These findings underscore the complementary roles of GFAP-positive cell counts and GFAP area in assessing astrogliosis. The observed profiles resemble those found in neurodegenerative and psychiatric disorders, raising the possibility of shared pathological mechanisms. Although functional outcomes were not directly assessed, these structural changes provide insight into METH-related brain alterations and highlight astrocytes as potential targets for therapeutic intervention.

Keywords: Methamphetamine, Striatum, Nucleus accumbens, Hippocampus, Astrocyte, Glial fibrillary acidic protein, Astrogliosis, Immunohistochemistry

Introduction

Methamphetamine (METH) is a highly addictive psychostimulant substance that potently affects the central nervous system. In addition to addiction, chronic METH abuse has many negative consequences, including psychotic symptoms and cognitive deficits. Accumulated data indicate that the striatum and hippocampus are key brain regions involved in drug addiction. The ventral striatum plays a critical role in

drug-seeking behaviour [1] and psychotic symptoms [2], whereas the dorsal striatum plays an important role in the development of compulsive behaviour and addiction [3]. The nucleus accumbens (NAc), in the ventral striatum, is known as a key node of reward circuitry and is involved in the distributed network of brain regions implicated in addiction [4]. Connections between the NAc and hippocampus were found to be associated with addiction-related behavior [5] and memory impairments after repeated exposure to amphetamine [6].

METH has been reported to disrupt neurotransmission with dopamine [7-10], serotonin [9-11] and glutamate [12]. It also has neurotoxic effects, notably the neuronal degeneration apparent in the striatum [13] and hippocampus [14]. As well as the extensive damage to neurotransmitter-producing neurons, there is growing evidence that neuroglial activity plays an essential role in the pathophysiology of drug-induced brain dysfunction [15,16]. Astrocytes are the most abundant neuroglia in the brain and play an important role in CNS homeostasis by regulating neurotransmitter release, buffering extracellular ions, and modulating neuronal activity. Astrocyte activation occurs with hypertrophy of cellular processes and upregulation of glial fibrillary acidic protein (GFAP), the principal intermediate filament protein in mature astrocytes in the CNS. This astrogliosis is involved in brain damage [17] and in the pathogenesis of neurodegenerative diseases [18,19]. Astrocyte dysfunction has also been implicated in several neurotoxic processes [20,21] as well as those associated with abused drugs [22,23]. Acute METH administration causes alteration in gene expression in primary cortical astrocytes [24]. Similarly, sub-acute METH administration alters the pattern of gene expression at the RNA level in primary striatal astrocytes [25]. Additionally, chronic METH treatment can cause cytotoxicity in differentiated C6 astroglia-like cells [26]. More recently, changes in astrocytic morphology in hippocampal tissue and elevated inflammatory marker proteins in the primary culture of hippocampal astrocytes were found after acute METH binge administration [27].

However, the neurotoxic effects of METH have been identified mainly from acute and/or high-dose regimens in laboratory animals. These drug administration paradigms do not closely mimic human patterns of stimulant abuse. A regimen including a gradual escalation of doses prior to multiple high-dose METH binge exposure exhibits dopaminergic-related effects and behavioral changes resembling those that occur as a consequence of METH abuse in humans [28]. Therefore, the present study aimed to determine the expression of astrocytes in rat brain regions associated with drug addiction circuity including the dorsal striatum, nucleus accumbens, cornu ammonis (CA) and dentate gyrus of the hippocampus, after METH exposure using this paradigm.

Materials and methods

Animals

This study was approved by the Animal Research Committee of Naresuan University (54 02 003). All animal procedures were conducted in accordance with the National Institutes of Health (USA) Guidelines for the treatment of laboratory animals. Also, this study was conducted in compliance with the ARRIVE guidelines. Twenty-one eight-week-old male Sprague-Dawley rats (mean weight ± SEM, 240.70 ± 3.06 g; National Animal Center, Salaya, Nakorn Pathom, Thailand) were housed individually in each cage under a 12-h light/dark cycle at 24 ± 1 °C with free access to water and food.

Drugs and experimental design

D-methamphetamine hydrochloride (Lipomed AG, Arlesheim, Switzerland), with permission from the Ministry of Public Health, was used for the experiment. Rats were divided into four groups as follows: sham control (n = 7), acute-METH binge (AB) (n = 6), escalating dose-METH (ED) (n = 4) and ED-METH binge (ED-Binge) (n = 4). The dosing regimens were adapted from Segal *et al.* [28]. All injections were administered intraperitoneally (i.p.) in a volume of 2 mL/kg. Rats in the sham control group (Sham) received saline injections three times per day at 3-h intervals for 14 consecutive days, followed by four saline injections at 2-h intervals on day 15. Rats in the AB group received saline injections for 14 days, identical to the sham protocol, and on day 15 were administered an acute binge regimen consisting of four successive METH injections (6 mg/kg per injection) at 2-h intervals. Rats in the ED group received three daily injections of METH at 3-h intervals for 14 days. The initial dose was 0.1

mg/kg per injection and was increased by 0.1 mg/kg with each injection. On day 15, rats received four successive saline injections at 2-h intervals instead of METH. Rats in the ED-Binge group underwent the same escalating-dose METH regimen as the ED group for 14 days, followed on day 15 by an acute binge regimen consisting of four successive METH injections (6 mg/kg per injection) at 2-h intervals. Saline-injected animals served as the sham control to account for handling and injection-related effects. Drug administration regimens are shown in **Figure 1(O)**. Twenty-four h after the final injection, all rats were euthanized by cervical dislocation for further investigation.

Astrocyte immunohistochemistry

Rat brains were collected 24 h after the last injection and preserved in 10% buffered formalin before being embedded in paraffin. The dorsal striatum (caudate and putamen), ventral striatum (nucleus accumbens), and hippocampus (CA regions and dentate gyrus) were sectioned at 5 μm according to the rat brain atlas at bregma 2.20 and −3.30 mm. Astrocytes were identified by immunoreactivity for GFAP, which served as the primary marker for assessing astrocytic activation in this study. The sections were deparaffinized, and antigens were retrieved by heating at high temperature in PBS. Sections were treated with endogenous peroxidase blocking solution containing PBS with 0.6% hydrogen peroxide, 0.1% Triton-X 100, 10% methanol for 1 h. Following washing with PBS, blocking reagent containing 5% normal serum in PBS was applied to the sections at room temperature for 2 h. Anti-GFAP primary antibody (MAB360; Sigma, USA) at a dilution of 1:1000 in a blocking solution was then applied to the sections for 1 h at room temperature. After washing with PBS, the sections were incubated with biotinylated secondary antibodies for 45 min. The sections were washed with PBS, and avidin biotinylated horseradish peroxidase complexes (Vectastain ABC kit, Vector Laboratories, CA) at a dilution of 1:100 in PBS were added to the sections for 30 min. Subsequently, the antigens were visualized using chromogen 3, 3-diaminobenzidine. Negative controls were performed by processing sections in parallel without the primary antibody to confirm the specificity of the immunohistochemical procedure.

Image analysis

Images were captured using a digital camera (DP21, Olympus) connected to a microscope (BX43, Olympus) at 10× magnification. The number of GFAP-positive cells was determined in dorsomedial (DSM) striatum, dorsolateral (DSL) striatum, NAc core (NAcC), NAc shell (NAcS), hippocampus CA1, CA2, CA3, and dentate gyrus (DG) subregions under identical acquisition settings for all samples to provide a broad view of each brain subregion. Regions of interest (ROIs) were defined based on anatomical landmarks, and images were acquired from comparable anatomical locations across all animals. Multiple non-overlapping fields within each region were selected in a systematic manner to minimize selection bias. All analyses were performed using image analysis software (ImageJ, US National Institutes of Health). The GFAP-positive cells were manually counted within predefined ROIs of fixed size. A 390×390 pixel ROI was used for hippocampal subregions, encompassing entire cellular layers, whereas a 1,000×1,000 pixel ROI was applied for the NAc and dorsal striatum. Quantification was performed using three sections per animal. Values were averaged per animal and used for statistical comparisons. For counting, selected ROIs were enlarged on-screen in ImageJ to improve visualization without altering the original image data, and identical viewing conditions were applied across all images. Astrocyte-like cells were identified and counted primarily based on GFAP immunoreactivity, which marks both the cytoplasmic and process elements of astrocytes [29,30]. Only GFAP-positive cells exhibiting distinctly defined soma and distinctive astrocytic morphology, including stellate, bipolar, or flat configurations, were included in the analysis [31,32]. Nevertheless, the combination of GFAP staining and morphological criteria allowed reliable identification of astrocytes across brain regions. Interpretation of astrocytic activation was further supported by qualitative morphological features, including hypertrophic soma and thickened processes, observed in GFAP-stained images.

We examined the accumulated area of GFAP-positive portions according to a method previously reported [33]. Briefly, the color images of GFAP immunohistochemistry stain were converted to binary images using image analysis software. The binary threshold was determined by comparing with the

original image; thus, astrocytes but not background staining could be recognized. The GFAP-positive portions were then measured and expressed as a ratio of the accumulated area of GFAP-positive portions to the entire area of interest studied. The values for each ROI for each animal were averaged and reported as the percentage area of GFAP-positive portions (GFAP%). All measurements were carried out blind to treatment.

Statistical analysis

Statistical analysis was performed using SPSS software (version 26.0. IBM Corp., Armonk, NY, USA). The normal distribution of the data was determined by the Shapiro-Wilk test. Data were analyzed using one-way ANOVA with post hoc Dunnett test. Data were reported as mean ± SEM. The statistical significance was determined as *p*-values less than 0.05.

Results and discussion

GFAP immunoreactivity in dorsal striatum, nucleus accumbens, and hippocampus

Staining for GFAP-positive cells in all regions in the present study showed morphological aspects of astrocyte-like cells. Sham animals presented with GFAP-positive cells in a resting-like state characterized by a mainly stellate shape, and some bipolar and flat cytoplasmic cells [31]. These GFAP-positive cells had small somata and thin, finely branched processes with non-overlapping domains, as demonstrated in the sham rat (**Figures 1(D)** - **1(F)** and **1(J)**). In contrast, METH-treated rats exhibited cellular hypertrophy, elongated and thickened processes (**Figures 1(A)** - **1(C)**, **1(K)** and **1(L)**), as well as some ramification and overlap with adjacent cell processes, which is consistent with astrogliosis. Negative controls, with the primary antibody omitted, showed no GFAP staining, confirming the specificity of the immunoreactivity (**Figures 1(G)** - **1(I)**). These morphological alterations were consistently observed alongside increased GFAP immunoreactivity in the dorsal striatum, NAc, and hippocampus (**Figures 2(C)** - **4(C)**), suggesting region-specific changes consistent with astrogliosis beyond GFAP upregulation alone. No specific GFAP immunoreactivity was observed in negative control sections processed without the primary anti-GFAP antibody, as demonstrated in **Figures 1(G)** - **1(I)**.

To quantify GFAP-positive areas, immunohistochemically stained images, such as **Figure 1(M)**, were converted into a binary format (**Figure 1(N)**). Threshold levels were adjusted by referencing the original images to ensure accurate detection of GFAP immunoreactivity while excluding background staining. This approach enabled consistent and reliable quantification of GFAP-positive signals.

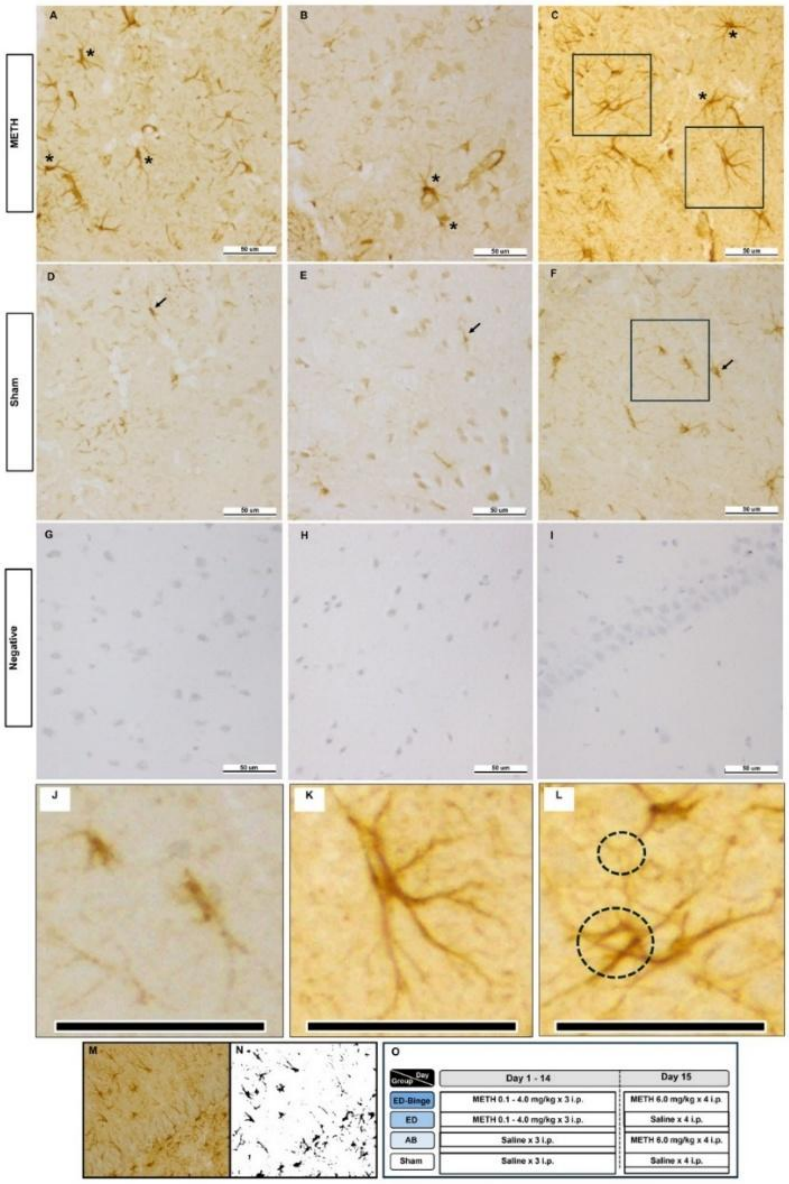

Figure 1 GFAP immunoreactivity in astrocytes across the striatum and hippocampus. Microscopic images show GFAP-positive cells, identified by dark brown staining, in the dorsal striatum (A,D), nucleus accumbens (B,E), and hippocampus (C,F). Morphological features of GFAP-positive cells are indicated, for example, by asterisks and arrows. GFAP immunostaining revealed that most astrocyte-like cells in the sham group exhibited a resting-like morphology (D-F), whereas features consistent with astrogliosis were observed in METH-treated rats, for example, in the ED-Binge group (A-C). Representative images were captured at 40× magnification. Insets cropped from the original images (C,F) are shown in panels (J-L), proportionally enlarged to highlight astrocytic morphology. Scale bar: 50 μm. Panel (J) shows a region from panel (F) illustrating resting-like morphology in the sham group, whereas panels (K) and (L) show regions from panel C illustrating features consistent with astrogliosis in the ED-Binge group. Panel (K) highlights cellular hypertrophy with elongated and thickened processes, while the circled area in panel (L) indicates overlapping GFAP-positive processes. Negative controls, without the primary anti-GFAP antibody, are shown in panels (G-I) for the dorsal striatum, nucleus accumbens, and hippocampus, respectively. No brown DAB staining is observed, only hematoxylin-stained nuclei, which were used solely to visualize cellular organization. Panel (M) shows a representative GFAP immunohistochemistry image that was converted into the binary image shown in panel (N) for analysis of GFAP-positive area. Panel (O) illustrates the drug administration regimens used in the study.

Quantitative analysis of GFAP-positive cells in the dorsal striatum

According to a quantitative analysis in the striatum as depicted in **Figure 2(A)**, one-way ANOVA revealed significant differences in the number of GFAP-positive cells in the dorsal striatum (p = 0.002), DSM (p = 0.006) and DSL (p = 0.001) subregions. Following Dunnett post-hoc analysis, significant elevations in the number of GFAP-positive cells were found in both the DSM (p = 0.005) and DSL (p = 0.0004) striatum in the ED-Binge group, reaching 169.7% and 191.4% of the sham group, respectively. The AB group also showed a significant increase in the number of GFAP-positive cells in the DSM striatum (p = 0.015).

Further analysis of GFAP% in the dorsal striatum (**Figure 2(B)**), a significant difference in GFAP% among the 4 groups was detected in both the DSM (p = 0.002) and DSL (p = 0.0001) striatum by one-way ANOVA. Dunnett post-hoc analysis showed an increase in GFAP% in the DSL in all METH groups versus the sham group (ED-Binge p = 0.00002, ED p = 0.016 and AB p = 0.025), whereas in the DSM striatum, an increased GFAP% was found in the ED-Binge (p = 0.005) and AB (p = 0.002) groups compared to the sham group.

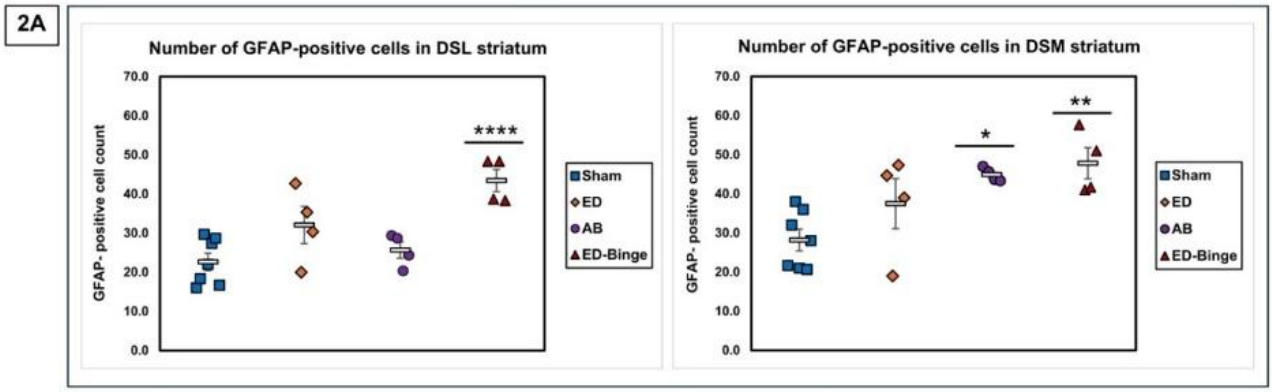

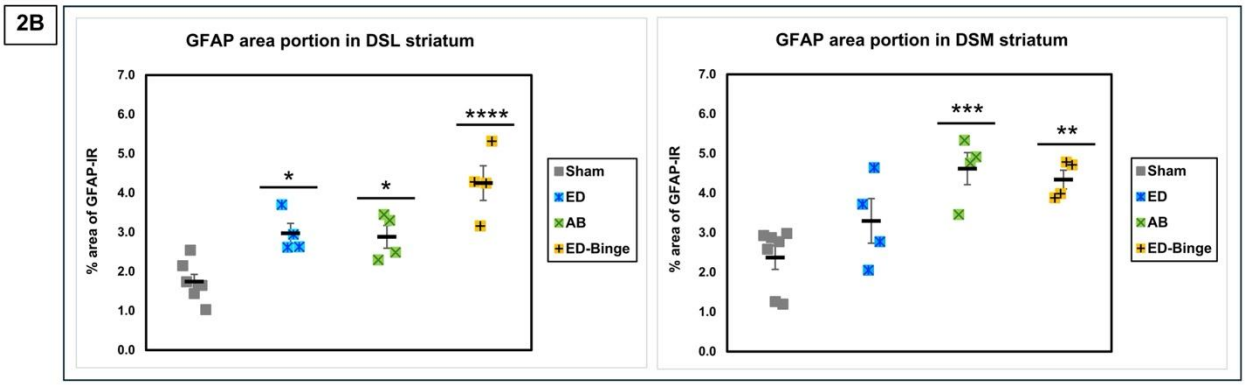

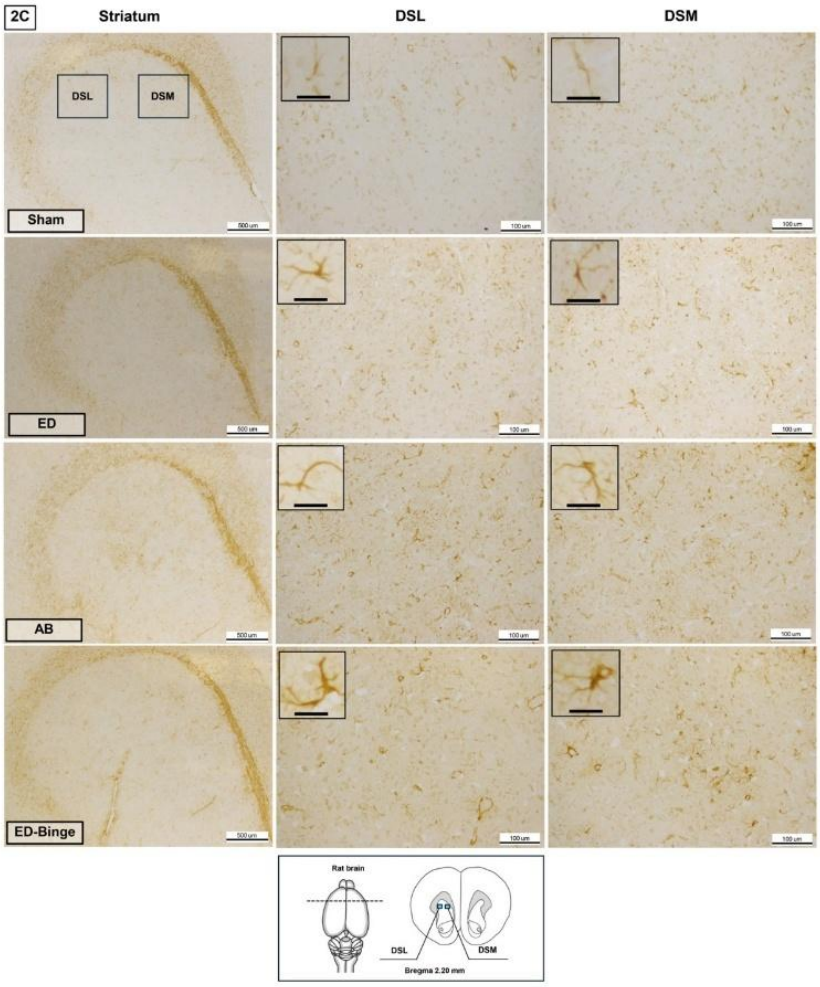

Figure 2 Investigation of GFAP immunoreactivity in striatal regions, dorsomedial (DSM) and dorsolateral (DSL) striatum, after METH administrations. The experimental groups included sham control (Sham), acute-METH binge (AB), escalating dose-METH (ED), and ED-METH binge (ED-Binge). (A) Demonstrating the number of GFAP-positive cells. Values represent mean ± SEM (n = 4 - 7). *$p < 0.05$, **$p < 0.01$, ****$p < 0.001$ in comparison with Sham by one-way ANOVA with Dunnett post-hoc test. (B) Demonstrating the percentage area of GFAP-positive portions. Values represent mean ± SEM (n = 4 - 7). *$p < 0.05$, **$p < 0.01$, ***$p < 0.005$, ****$p < 0.001$ in comparison with Sham by one-way ANOVA with Dunnett post-hoc test. (C) Representative images of GFAP immunostaining in the dorsal striatum. Experimental groups are arranged from top to bottom (Sham, METH-treated). Images at 4× magnification (left panel; scale bar = 500 μm) show the overall dorsal striatum, whereas 20× magnification images (middle and right panels; scale bar = 100 μm) display the DSL and DSM subregions, respectively. Insets in the middle and right panels show GFAP-positive cell morphology at 40× magnification (scale bar = 50 μm).

Quantitative analysis of GFAP- positive cells in the nucleus accumbens

Following one-way ANOVA, there were significant differences in the number of GFAP-positive cells among the four groups in the NAc ($p = 0.0007$), NAcC ($p = 0.0003$) and NAcS ($p = 0.009$). Dunnett post-hoc (**Figure 3(A)**) showed an elevated number of GFAP-positive cells in the NAcC of the ED ($p = 0.002$), AB ($p = 0.001$), and ED-Binge ($p = 0.001$) groups compared to the Sham group. For the NAcS, increases were significant in the ED ($p = 0.005$) and ED-Binge ($p = 0.04$) groups but not in the AB group. Further quantitative analysis showed no significant difference of GFAP% ($p = 0.058$) in the NAcS by one-way ANOVA (**Figure 3(B)**). Although GFAP% increased to 184.1% ($p = 0.059$) in the ED group and 180.4% ($p = 0.073$) in the ED-Binge group, Dunnett post-hoc test revealed no statistically significant differences compared to the Sham group.

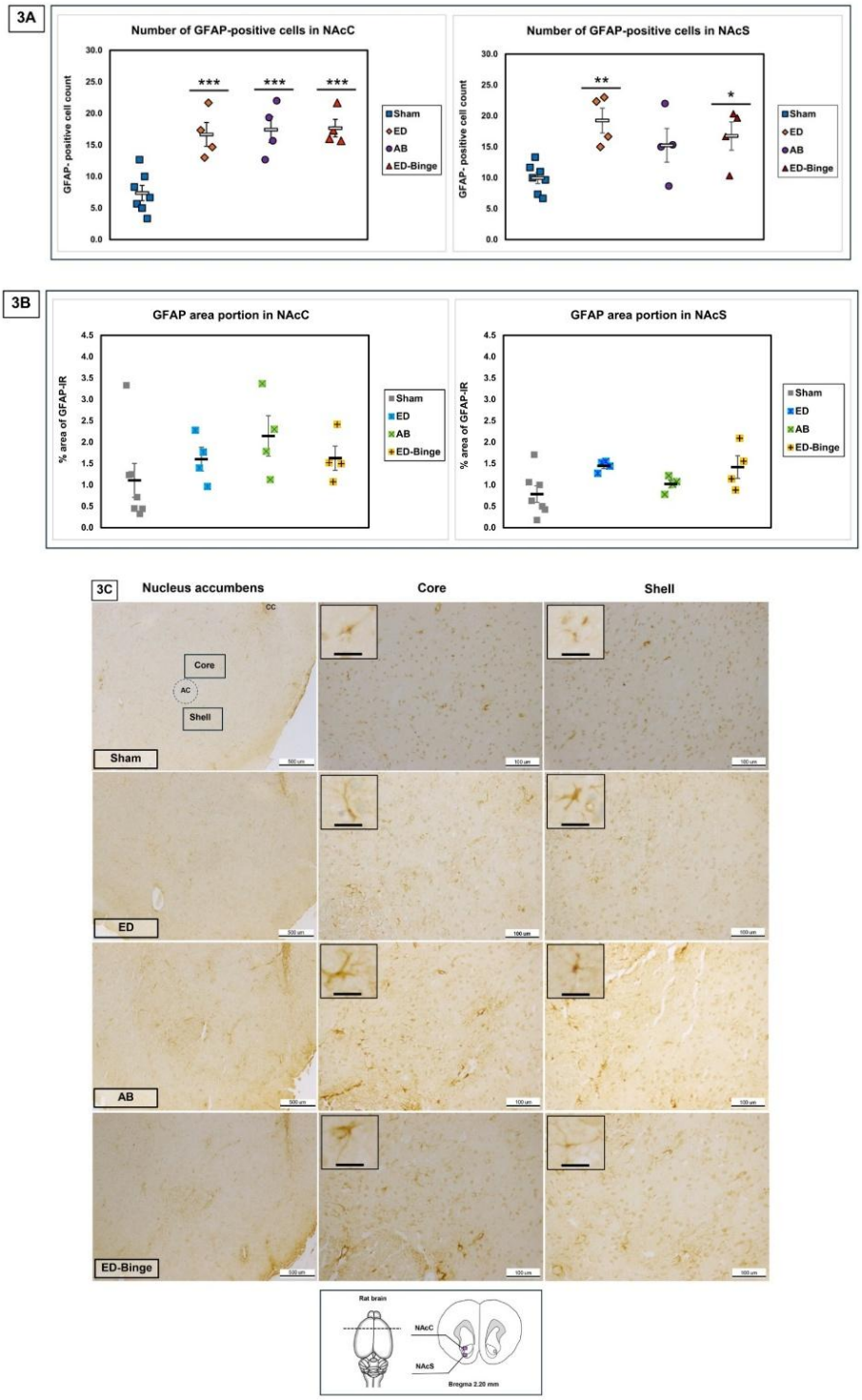

Figure 3 Investigation of GFAP immunoreactivity in nucleus accumbens (NAc), NAc core (NAcC) and NAc shell (NAcS), after METH administrations. The experimental groups included sham control (Sham), acute-METH binge (AB), escalating dose-METH (ED), and ED-METH binge (ED-Binge). (A) Demonstrating the number of GFAP-positive cells. Values represent mean ± SEM (n = 4 - 7). *$p < 0.05$, **$p < 0.01$, ***$p < 0.005$ in comparison with Sham by one-way ANOVA with Dunnett post-hoc test. (B) Demonstrating the percentage area of GFAP-positive portions. Values represent mean ± SEM (n = 4 - 7). (C) Representative images of GFAP immunostaining in the nucleus accumbens (NAc). Experimental groups are arranged from top to bottom (Sham, METH-treated). Images at 4× magnification (left panel; scale bar = 500 µm) show the overall NAc, whereas 20× magnification images (middle and right panels; scale bar = 100 µm) display the NAcC and NAcS subregions, respectively. Insets in the middle and right panels show GFAP-positive cell morphology at 40× magnification (scale bar = 50 µm). AC, anterior commissure; CC, corpus callosum.

Quantitative analysis of GFAP- positive cells in the hippocampus

One-way ANOVA followed by Dunnett post hoc analysis in the hippocampus showed a significant increase in the number of GFAP-positive cells only in the CA2 of the ED group compared to the Sham group (p = 0.048), whereas significant differences were not detected in the CA1, CA3 and dentate gyrus (**Figure 4(A)**). Further quantitative analysis of GFAP% revealed significant differences across all hippocampal regions (**Figure 4(B)**). The GFAP% after ED-Binge exposure was significantly higher than that of the Sham in all hippocampal regions (CA1 p = 0.00004, CA2 p = 0.00007, CA3 p = 0.001, and dentate gyrus p = 0.0004). Moreover, the AB group showed a significant increase in GFAP% in the CA2 (p = 0.034) and CA3 (p = 0.027).

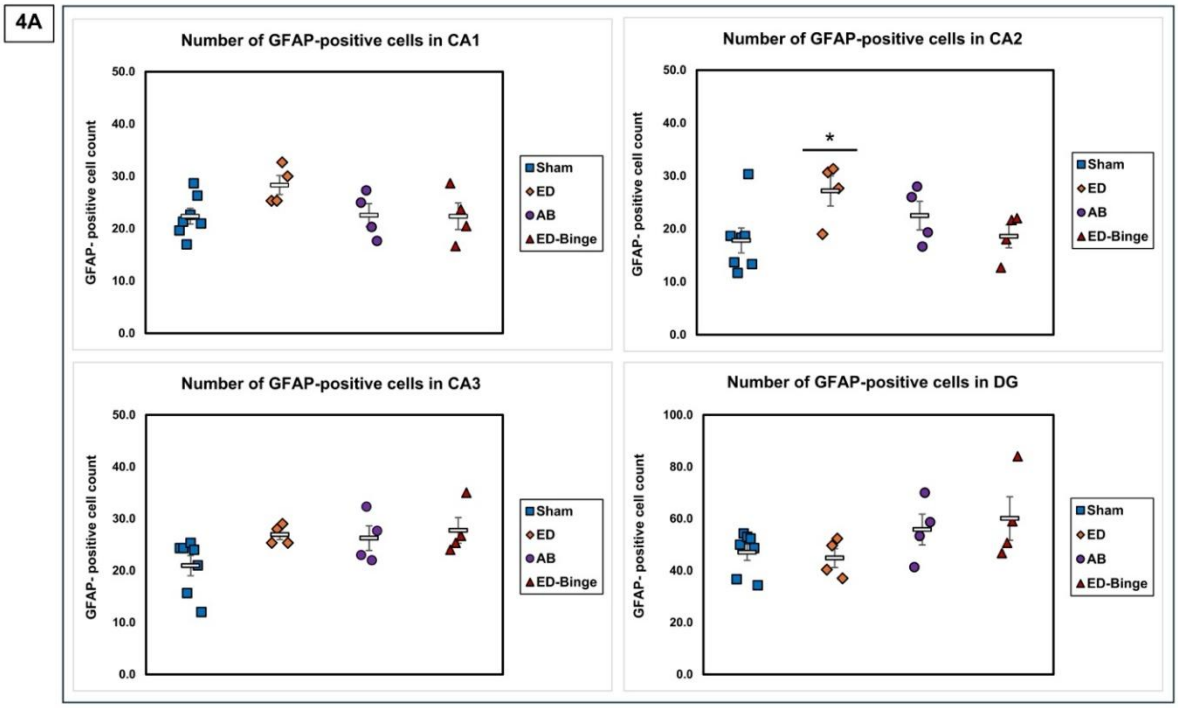

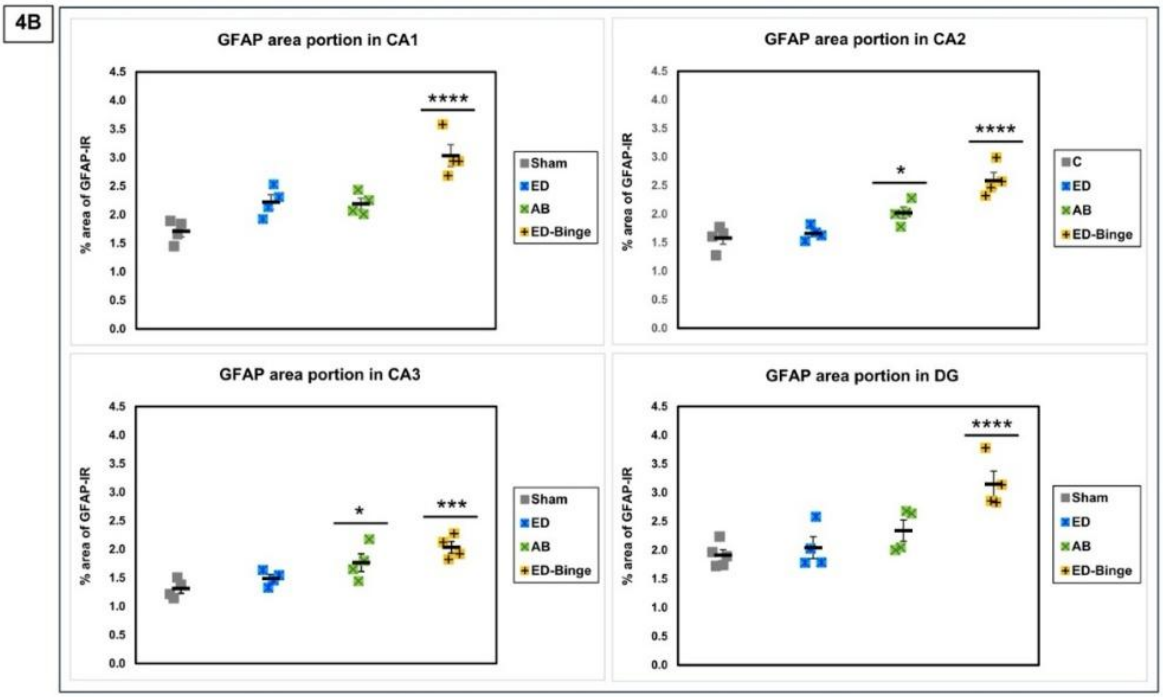

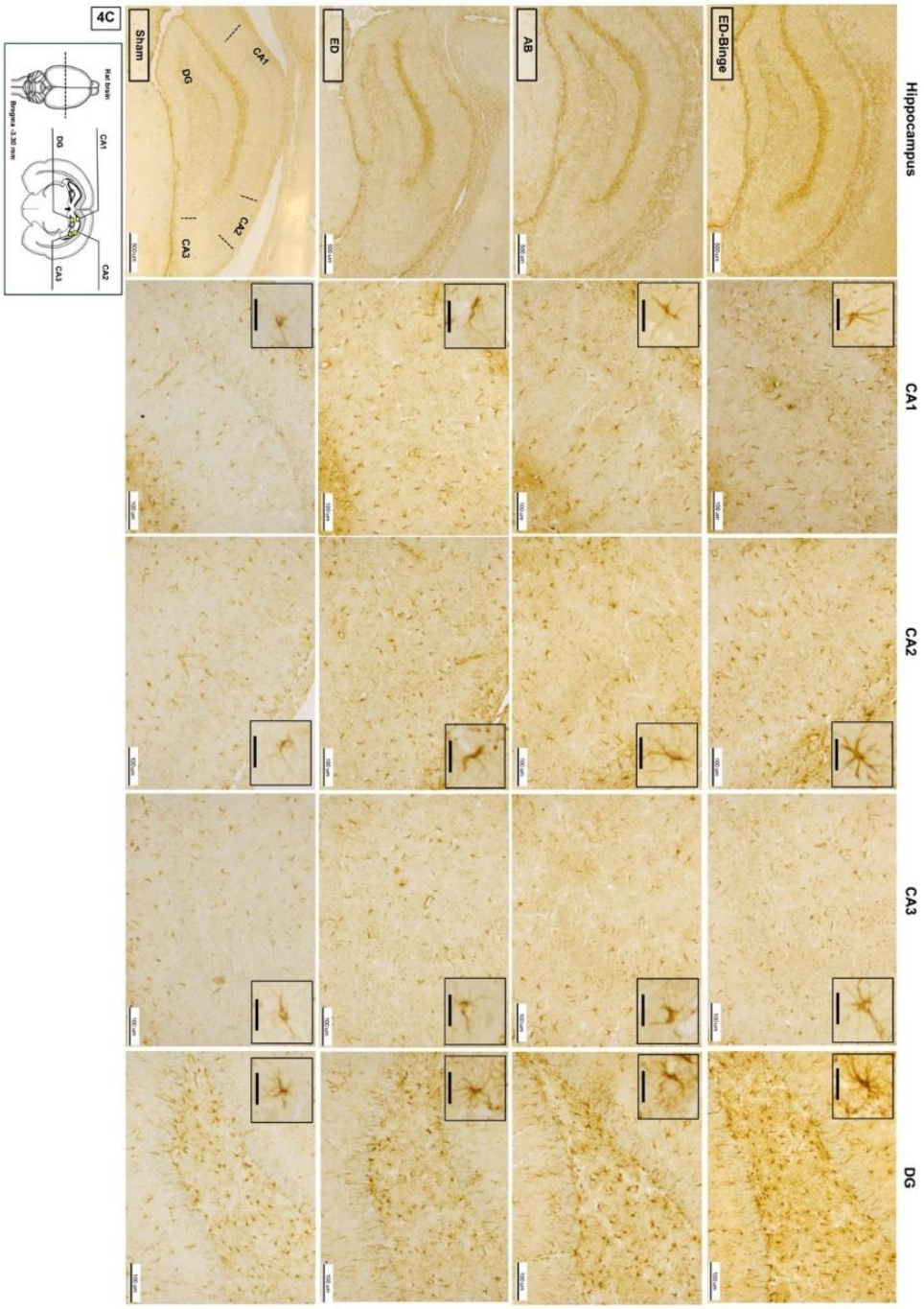

Figure 4 Investigation of GFAP immunoreactivity in hippocampus cornu ammonis (CA)1, CA2, CA3 and dentate gyrus (DG) subregions after METH administrations. The experimental groups included Sham, acute-METH binge (AB), escalating dose-METH (ED), and ED-METH binge (ED-Binge). (A) Demonstrating the number of GFAP-positive cells. Values represent mean ± SEM (n = 4 - 7). *$p < 0.05$ in comparison with Sham by one-way ANOVA with Dunnett post-hoc test. (B) Demonstrating the percentage area of GFAP-positive portions. Values represent mean ± SEM (n = 4 - 5). *$p < 0.05$, ***$p < 0.005$, ****$p < 0.001$ in comparison with Sham by one-way ANOVA with Dunnett post-hoc test. (C) Representative images of GFAP immunostaining in the hippocampus. Experimental groups are arranged from left to right (Sham, METH-treated). The top panel (4× magnification; scale bar = 500 µm) shows an overview of the hippocampus. The middle and lower panels (20× magnification; scale bar = 100 µm) show the hippocampal subregions CA1, CA2, CA3, and DG arranged in separate horizontal rows beneath the top panel. Insets within the subregion panels show GFAP-positive cell morphology at 40× magnification (scale bar = 50 µm).

The primary finding of the present study was a marked increase in GFAP immunoreactivity, suggestive of astrogliosis, following METH administration in the dorsal striatum, NAc, hippocampal CA and dentate gyrus subregions. This response was characterized by increased GFAP immunoreactivity and observable morphological changes consistent with astrocyte reactivity, including enlarged somata and thickened processes. While GFAP alone does not encompass the full complexity of astrogliosis, it remains a widely accepted and sensitive marker of early or mild astrocytic activation, especially in the context of subtle neurotoxic insults without overt tissue damage [21,34]. Importantly, our morphological observations provide qualitative evidence of reactive changes beyond GFAP expression alone, although we did not include proliferation markers in the current study. The patterns of astrocyte reactivity observed in this study are consistent with previous findings in models of neurotoxicity and neuroinflammation, including Parkinson's disease, Alzheimer's disease, as well as traumatic brain injuries, where GFAP upregulation and astrocytic hypertrophy have been reported as hallmark features of reactive gliosis [17,35-38]. Our results suggest that METH administration in rats modeling human METH abuse patterns exerts deleterious effects on both dopaminergic and non-dopaminergic brain regions, consistent with its broad neurotoxic profile.

While GFAP is a widely accepted marker of astrocytic reactivity, it does not fully capture the complex neurotoxic effects of METH. Complementary data from our laboratory using the same rat METH exposure model have demonstrated broader neurochemical changes, including region-specific alterations in hippocampal brain-derived neurotrophic factor [39] and calcium-binding proteins involved in neuronal function in the frontal cortex and hippocampus [40]. These neurochemical changes suggest that METH induces a cascade of neuronal dysfunction, including impaired neurotrophic support and calcium homeostasis, which likely contributes to the astrocytic reactivity observed in our study. Taken together, these findings support a broader interpretation of METH-induced neurotoxicity that involves both neuronal and glial components, contributing to reactive astrogliosis. Additionally, METH exposure disrupts hippocampal neurogenesis by altering neuronal differentiation, potentially exacerbated by decreased blood-brain barrier integrity and neuroinflammation [41-44]. Although these findings demonstrate structural and molecular alterations in the hippocampus, further studies incorporating functional and behavioral assessments are needed to better understand the consequences of these changes.

Notably, the ED-Binge regimen, which mimics human abuse patterns, induced pronounced astrocytic reactivity in the dorsal striatum and hippocampus. The heightened vulnerability of these regions underscores their susceptibility to METH-induced neurotoxicity, potentially disrupting motor control, memory consolidation, and cognitive function. Furthermore, we observed region-specific astrocytic responses to METH exposure. The NAcC exhibited sensitivity across all dosing regimens, whereas the NAcS was predominantly affected by chronic regimens (escalating-dose and escalating dose-binge). Given the established role of the NAc in reward circuitry and addiction [4], our findings align with the hypothesis that the NAcC and NAcS have distinct yet interrelated functions in the context of METH addiction. The NAcC demonstrated a rapid response and was sensitive to both acute and chronic stimulant exposure, while the NAcS appeared to be more involved in long-term neuroadaptive processes associated with chronic METH use. These findings align with accumulating evidence that METH exposure disrupts neuronal function and engages neuroinflammatory signaling within reward circuitry, including the NAc, accompanied by glial activation characterized by microglial activation and astrocytic dysregulation that may contribute to cellular stress and maladaptive neuroplasticity [45-47]. Moreover, the findings reinforce the notion that the NAc core, rather than the shell, plays a pivotal role in mediating addiction-related behaviors, such as METH craving [48]. Consistent with prior evidence of core-specific involvement in craving incubation, persistent synaptic adaptations within the NAcC have been associated with METH craving [49]. On the other hand, research has implicated the NAcS in influencing behavioral responses to continuous exposure to rewarding stimuli, such as chronic drug administration [50].

Different astrocyte responses are observed with the various METH dosing regimens. ED-Binge regimens dramatically increased astrogliosis more than ED and AB alone. As levels of GFAP have been proposed as a potential biomarker of disease severity [51,52], the recent observation of a significant increase in GFAP may indicate increased vulnerability to brain damage after ED-Binge exposure. Although administering escalating dose-daily METH prior to a multiple high-dose METH binge reduced hyperthermia and stereotypy as well as prevented dopamine and dopamine transporter loss in the striatum, it did not reverse other dopamine elements [28]. Additionally, in METH users, neuronal degeneration has been found in both dopamine- and nondopamine-innervated regions [53,54], as has also been observed in the frontal cortex and hippocampus of rats treated with the ED-Binge regime [55].

Moreover, our findings revealed region-specific astrocytic responses to METH. In the ED group, CA2 showed increased astrocyte numbers without a significant change in GFAP area, indicating mild activation with limited cytoskeletal remodeling. In contrast, the ED-Binge group exhibited increased GFAP area in CA1, CA2, CA3, and DG without an increase in GFAP-positive cells, suggesting hypertrophy or process elongation. These findings reflect astrocyte reactivity, which is complicated and dose-dependent. These findings illustrate the complicated and dose-dependent characteristics of astrocyte reactivity. The present study demonstrates astrocytic reactions to METH throughout various hippocampal subregions, highlighting its different neurotoxic consequences. This provides a significant basis for forthcoming functional and behavioral investigations concerning subregional vulnerability.

Interestingly, region-specific differences were observed, apparent in the NAcC across all METH-treated groups, the NAcS in the ED group, and the CA2 in the ED group, where astrocyte numbers increased without a corresponding expansion of GFAP-positive area. This may reflect early or mild astrocytic activation with limited cytoskeletal remodeling [32,34,56], emphasizing the importance of using cell counts and GFAP area as complementary indicators of gliosis. Conversely, the dorsolateral striatum in the AB and ED groups, but not ED-Binge, showed increased GFAP-positive area without a rise in GFAP-positive cell number, suggesting hypertrophy or process elongation rather than proliferation [32,57,58]. This supports the interpretation that astrocyte number and GFAP area reflect distinct, complementary aspects of reactivity.

Dysfunction in brain networks associated with the striatum has been elucidated as a mechanism underlying addiction [59]. The striatum receives glutamatergic and dopaminergic projections from multiple brain regions, including the cortex, hippocampus, and ventral tegmental area, and is implicated in regulating the development and maintenance of addiction [60,61]. Neuronal activity of afferent input can be conveyed from the NAcS, through NAcC, and subsequently into the dorsal striatum [61,62]. Further activity shifting from the DSM to DSL striatum has been discovered in rats with prolonged alcohol exposure, suggesting that drug seeking transforms into habitual behavior involved in addiction [63]. The current findings of maladaptive astrocytes may imply dysfunctional connectivity in the striatal sub-region. Disruption of neuronal signaling occurs in both the striatum and the hippocampus, as dysregulated glutamate reuptake was detected in both the striatum and hippocampus after exposure to METH and alcohol [64].

METH exposure causes neurotoxicity [13,14,65,66], and an astrocytic response to METH is implicated in METH-induced neurotoxicity. In the hippocampus of rats receiving METH, reactive astrocytes promoted the neurotoxic factor lipocacin-2, which produced neuronal death through mitochondrion-related apoptosis or neuroinflammation via microglial activation [67]. Neuroinflammation has been implicated as a mechanism of METH-induced neurotoxicity, as METH can induce the astrocytic release of proinflammatory cytokines, which then produce microglia activation, promoting neuroinflammation [68]. Astrocytic and neuroinflammatory changes may contribute to the widespread neurotransmission disruptions reported in METH-induced neuropathology. METH has been found to disrupt neurotransmission in several brain areas, including the striatum, NAc, cerebral cortex, ventral tegmental area, and hippocampus, often accompanied by nerve terminal degeneration or cell death [28,66,69,70]. In our study, astrogliosis was observed in the striatum, NAc, and hippocampus, suggesting that glial responses may

contribute to broader neural changes induced by METH. Although no direct functional or behavioral assessments were conducted, the presence of astrogliosis in these regions may be consistent with neuropathological features reported in disorders such as schizophrenia [18] and Alzheimer's disease [71,72]. Such astrocytic responses in METH-exposed brains resemble patterns seen in neurodegenerative and psychiatric disorders, highlighting their potential relevance in METH-induced neuropathology.

Astrocytes are thought to play an important function in regulating glutamate uptake and minimizing excitotoxicity. Previous studies demonstrate that METH rapidly increases extracellular glutamate through astrocytic glutamate release [68], and that sustained glutamate elevation arises from impaired astrocytic glutamate clearance during withdrawal [73]. This was supported by previous findings of downregulated expression of glutamate transporter EAAT2, the major glutamate reuptake mechanism, which is expressed mainly on astrocytes, in the striatum and hippocampus after METH binge administration [64]. In addition, reactive astrogliosis in pathological conditions has been associated with reduced EAAT2 expression and impaired glutamate uptake. For example, a recent study in postmortem brain tissue from patients with the parkinsonian type of multiple system atrophy demonstrated increased GFAP-positive astrocytes along with reduced EAAT2 expression and altered subcellular localization, contributing to glutamate dysregulation and excitotoxic vulnerability [74]. These findings support the notion that astrocytic structural changes observed in our METH model could likewise contribute to affect glutamate clearance, although transporter function was not directly assessed in the present study. Besides glutamate, METH disrupts the dopaminergic system by depleting striatal dopamine following either binge or ED-binge exposure [28]. Astrocytes also have an influence on dopamine transmission, as indicated by the downregulation of dopamine transporter and dopamine receptor DRD2 gene expressions in cultured primary astrocytes subsequent to METH treatment [75]. Given the role of astrocytes in structural support and neurotransmitter homeostasis, the observed increase in astrocyte number and morphological changes in our study may reflect a response to METH-induced neurotoxicity, potentially linked to maladaptive neurotransmission. However, further studies are needed to directly assess functional consequences.

The study has some limitations. In order to minimize both animal and drug use, sample sizes were small and, in the AB group, were further reduced by two animals dying from an acute toxic reaction. However, all rats in the ED and ED-Binge groups survived, which is consistent with other reports in the literature, and results with these small group sizes still yielded highly significant findings. GFAP expression was determined using immunohistochemical measures and is therefore limited as an indirect and semiquantitative assessment of protein levels. GFAP immunostaining primarily reflects reactive astrocytes and may not represent the entire astrocyte population. Therefore, the findings should be interpreted as changes in GFAP-associated reactivity rather than absolute alterations in total astrocyte number. Nevertheless, the observed morphological changes and increased GFAP immunoreactivity are suggestive of, and consistent with, astrogliosis following METH treatment.

Conclusions

In conclusion, METH administration at doses that closely resemble human patterns of METH abuse induces widespread increases in GFAP immunoreactivity, suggestive of astrogliosis, in key brain regions implicated in addiction, memory processing, and cognitive function, including the striatum and hippocampus. The observed astrocytic reactivity, characterized by elevated GFAP-positive immunoreactivity, suggests a potential role for astrocytes in METH-induced neurotoxicity. The patterns observed in this study are comparable to those reported in schizophrenia and neurodegenerative diseases, indicating a possible pathological correlate for the psychosis, cognitive and learning impairments that frequently accompany METH abuse. These findings emphasize the potential of targeting astrocytic-related responses in developing therapeutic strategies for METH-induced neurotoxicity and associated negative consequences.

Acknowledgements

This research was supported by Naresuan University, Thailand, Research Fund (grant number R2556B067). This work was partially supported by

Naresuan University, Thailand: Fundamental Fund (grant number R2567B022), School of Medical Sciences, University of Phayao, Thailand (grant number MS-201015), Global and Frontier Research University Fund, Naresuan University, Thailand (grant number R2567C003) and Frontier Research and Innovation Clusters Grant (grant number R2569C004). We appreciate the facility support from the School of Medical Sciences, University of Phayao, Thailand and the Faculty of Medical Science, Naresuan University, Thailand.

Declaration of Generative AI in Scientific Writing

Generative AI tools were used to assist in language editing and improving readability. The authors accept full responsibility for the content and accuracy of the manuscript. QuillBot (Grammar checker and paraphrasing tool, version v32.19.3, QuillBot Inc.) was used to assist in language editing and to improve the readability of the manuscript. The authors take full responsibility for the content and the accuracy of the manuscript.

CRediT Author Statement

Walailuk Kerdsan-Phusan: Methodology; Investigation; Visualization; Formal analysis; Writing - Original draft; Writing - Review & Editing. **Samur Thanoi:** Conceptualization; Resources; Supervision; Writing - Review & Editing. **Gavin P Reynolds:** Conceptualization; Supervision; Writing - Review & Editing. **Sutisa Nudmamud-Thanoi:** Conceptualization; Funding acquisition; Resources; Project administration; Writing - Review & Editing.

References

[1] Y Li, X Zheng, C Gao, S Li, Z Liu, M Lv, F Xiao and Y Bai. Higher levels of D2R and D3R in the frontal-striatal regions are associated with reduced perseverative reward seeking after opioid abstinence. *Frontiers in Behavioral Neuroscience* 2025; **19**, 1552055.

[2] K Schmack, M Bosc, T Ott, JF Sturgill and A Kepecs. Striatal dopamine mediates hallucination-like perception in mice. *Science* 2021; **372(6537)**, eabf4740.

[3] L Marti-Prats, C Giuliano, A Domi, M Puaud, Y Pena-Oliver, M Fouyssac, C McKenzie, BJ Everitt and D Belin. The development of compulsive coping behavior depends on dorsolateral striatum dopamine-dependent mechanisms. *Molecular Psychiatry* 2023; **28(11)**, 4666-4678.

[4] Y Xu, Y Lin, M Yu and K Zhou. The nucleus accumbens in reward and aversion processing: Insights and implications. *Frontiers in Behavioral Neuroscience* 2024; **18**, 1420028.

[5] AL Eagle, C Sugimoto, MA Doyle, D Anderson, SL Mousavi, MM Dykstra, HM Kuhn, BR Murray, RM Bastle, S Simmons, J He, I Maze, MS Mazei-Robison and AJ Robison. Transcriptional regulation of ventral hippocampus-nucleus accumbens circuit excitability drives cocaine seeking. *Science Advances* 2026; **12(10)**, eadv1236.

[6] RJ McDonald, NS Hong, A Atwood, AV Tyndall and B Kolb. An assessment of the functional effects of amphetamine-induced dendritic changes in the nucleus accumbens, medial prefrontal cortex, and hippocampus on different types of learning and memory function. *Neurobiology of Learning and Memory* 2021; **180**, 107408.

[7] LM Lin, M Febo, AW Bruijnzeel, L Phan, A Gopinath, J Seibold, E Miller and H Khoshbouei. TNF-α signaling mediates the dopaminergic effects of methamphetamine by stimulating dopamine transporters and L-type Ca^{2+} channels. *Science Signaling* 2025; **18(917)**, eady8676.

[8] CM Chandler, JR Nickell, AG Wilson, JP Culver, PA Crooks, MT Bardo and LP Dwoskin. Vesicular monoamine transporter-2 inhibitor JPC-141 prevents methamphetamine-induced dopamine toxicity and blocks methamphetamine self-administration in rats. *Biochemical Pharmacology* 2024; **228**, 116189.

[9] MR Stocco, AA El-Sherbeni, B Zhao, M Novalen and RF Tyndale. The role of CYP2D in rat brain in methamphetamine-induced striatal dopamine and serotonin release and behavioral sensitization. *Psychopharmacology* 2021; **238(7)**, 1791-1804.

[10] Y Peng, Y Wang, L Liu, G Yang, D Zhang, S Hong and L Li. The effects of ketamine and methamphetamine on neurotransmitters, glutamate receptors, and conditioned place preference in rat. *Legal Medicine* 2023; **65**, 102328.

[11] B Čechová, J Jurčovičová, I Petríková, Š Vaculín, Š Šandera and R Šlamberová. Impact of altered environment and early postnatal methamphetamine exposure on serotonin levels in the rat hippocampus during adolescence. *Laboratory Animal Research* 2024; **40(1)**, 1.

[12] T He, N Li, P Shi, X Xu, J Nie, X Lu, P Yu, Y Fan, F Ge and X Guan. Electroacupuncture alleviates spatial memory deficits in METH withdrawal mice by enhancing astrocyte-mediated glutamate clearance in the dCA1. *Addiction Biology* 2022; **27(1)**, e13068.

[13] T He, C Han, C Liu, J Chen, H Yang, L Zheng, JL Waddington and X Zhen. Dopamine D1 receptors mediate methamphetamine-induced dopaminergic damage: involvement of autophagy regulation via the AMPK/FOXO3A pathway. *Psychopharmacology* 2022; **239(3)**, 951-964.

[14] B Yang, X Tan, Y Chen, J Lin, J Liang, X Yue, D Qiao, H Wang and S Du. The neuroprotective effects of caffeic acid phenethyl ester against methamphetamine-induced neurotoxicity. *Ecotoxicology and Environmental Safety* 2024; **279**, 116497.

[15] Y Tizabi, B Getachew, SR Hauser, V Tsytsarev, AC Manhães and VDA da Silva. Role of Glial Cells in Neuronal Function, Mood Disorders, and Drug Addiction. *Brain Sciences* 2024; **14(6)**, 558.

[16] S Shi, T Chen and M Zhao. The crosstalk between neurons and glia in methamphetamine-induced neuroinflammation. *Neurochemical Research* 2022; **47(4)**, 872-884.

[17] S Ramirez, A Mukherjee, S Sepulveda, A Becerra-Calixto, N Bravo-Vasquez, C Gherardelli, M Chavez and C Soto. Modeling traumatic brain injury in human cerebral organoids. *Cells* 2021; **10(10)**, 2683.

[18] T Sarkar, N Patro and IK Patro. Perinatal exposure to synergistic multiple stressors leads to cellular and behavioral deficits mimicking Schizophrenia-like pathology. *Biology Open* 2022; **11(3)**, bio058870.

[19] W Pelkmans, M Shekari, A Brugulat-Serrat, G Sanchez-Benavides, C Minguillon, K Fauria, JL Molinuevo, O Grau-Rivera, A Gonzalez Escalante, G Kollmorgen, M Carboni, NJ Ashton, H Zetterberg, K Blennow, M Suarez-Calvet and JD Gispert. Astrocyte biomarkers GFAP and YKL-40 mediate early Alzheimer's disease progression. *Alzheimer's & Dementia* 2024; **20(1)**, 483-493.

[20] B Li, M Xia, R Zorec, V Parpura and A Verkhratsky. Astrocytes in heavy metal neurotoxicity and neurodegeneration. *Brain Research* 2021; **1752**, 147234.

[21] DS Bouvier, S Fixemer, T Heurtaux, F Jeannelle, KBM Frauenknecht and M Mittelbronn. The multifaceted neurotoxicity of astrocytes in ageing and age-related neurodegenerative diseases: A translational perspective. *Frontiers in Physiology* 2022; **13**, 814889.

[22] GI Gómez, TF Alvear, DA Roa, A Farias-Pasten, SA Vergara, LA Mellado, CJ Martinez-Araya, J Prieto-Villalobos, C García-Rodríguez, N Sánchez, JC Sáez, FC Ortíz and JA Orellana. Cx43 hemichannels and panx1 channels contribute to ethanol-induced astrocyte dysfunction and damage. *Biological Research* 2024; **57(1)**, 15.

[23] W Yin, M Fandaros, Y Liu, R Lei, G Pittas, S Lee, Y Pan, DA Rubenstein and C Du. Cocaine affects astrocyte iNOS expression. *Brain Research* 2026; **1870**, 150068.

[24] N Bortell, L Basova, S Semenova, HS Fox, T Ravasi and MC Marcondes. Astrocyte-specific overexpressed gene signatures in response to methamphetamine exposure *in vitro*. *Journal of Neuroinflammation* 2017; **14(1)**, 49.

[25] T Wang, SQ Wu, XH Tan, CX Chen, X Yue, HJ Wang, SH Du and DF Qiao. Transcriptomic changes of astrocytes in the brain of rats with subacute METH exposure. *Fa Yi Xue Za Zhi* 2021; **37(6)**, 806-812.

[26] RB Badisa, C Wiley, K Randell, SF Darling-Reed, LM Latinwo, M Agharahimi, KFA Soliman and CB Goodman. Identification of cytotoxic markers in methamphetamine treated rat C6 astroglia-like cells. *Scientific Reports* 2019; **9(1)**, 9412.

[27] RA Leitão, CA Fontes-Ribeiro and AP Silva. The effect of parthenolide on methamphetamine-induced blood-brain barrier and astrocyte alterations. *European Journal of Clinical Investigation* 2022; **52(4)**, e13694.

[28] DS Segal, R Kuczenski, ML O'Neil, WP Melega and AK Cho. Escalating dose methamphetamine

pretreatment alters the behavioral and neurochemical profiles associated with exposure to a high-dose methamphetamine binge. *Neuropsychopharmacology* 2003; **28(10)**, 1730-1740.

[29] BD Dufour, T Bartley, E McBride, E Allen, YA McLennan, RJ Hagerman and V Martínez-Cerdeño. FXTAS neuropathology includes widespread reactive astrogliosis and white matter specific astrocyte degeneration. *Annals of Neurology* 2024; **95(3)**, 558-575.

[30] B Mota, AR Bras, L Araujo-Andrade, A Silva, PA Pereira, MD Madeira and A Cardoso. High-caloric diets in adolescence impair specific GABAergic subpopulations, neurogenesis, and alter astrocyte morphology. *International Journal of Molecular Sciences* 2024; **25(10)**, 5524.

[31] I Macikova, A Perzelova, P Mraz, I Bizik and J Steno. GFAP-positive astrocytes are rare or absent in primary adult human brain tissue cultures. *Biologia* 2009; **64(4)**, 833-839.

[32] A Verkhratsky, A Butt, B Li, P Illes, R Zorec, A Semyanov, Y Tang and MV Sofroniew. Astrocytes in human central nervous system diseases: A frontier for new therapies. *Signal Transduction and Targeted Therapy* 2023; **8(1)**, 396.

[33] S Wakasa, N Shiiya, T Tachibana, T Ooka and Y Matsui. A semiquantitative analysis of reactive astrogliosis demonstrates its correlation with the number of intact motor neurons after transient spinal cord ischemia. *Journal of Thoracic and Cardiovascular Surgery* 2009; **137(4)**, 983-990.

[34] C Escartin, E Galea, A Lakatos, JP O'Callaghan, GC Petzold, A Serrano-Pozo, C Steinhäuser, A Volterra, G Carmignoto, A Agarwal, NJ Allen, A Araque, L Barbeito, A Barzilai, DE Bergles, G Bonvento, AM Butt, WT Chen, M Cohen-Salmon, …, A Verkhratsky. Reactive astrocyte nomenclature, definitions, and future directions. *Nature Neuroscience* 2021; **24(3)**, 312-325.

[35] H An, H Lee, S Yang, W Won, CJ Lee and MH Nam. Adenovirus-induced reactive astrogliosis exacerbates the pathology of Parkinson's disease. *Experimental Neurobiology* 2021; **30(3)**, 222-231.

[36] A Kumar, IC Fontana and A Nordberg. Reactive astrogliosis: A friend or foe in the pathogenesis of Alzheimer's disease. *Journal of Neurochemistry* 2023; **164(3)**, 309-324.

[37] Y Yuan, H Liu, Z Dai, C He, S Qin and Z Su. From physiology to pathology of astrocytes: Highlighting their potential as therapeutic targets for CNS injury. *Neuroscience Bulletin* 2025; **41(1)**, 131-154.

[38] C Munoz-Ballester and S Robel. Astrocyte-mediated mechanisms contribute to traumatic brain injury pathology. *WIREs Mechanisms of Disease* 2023; **15(5)**, e1622.

[39] S Iamjan, S Veerasakul, GP Reynolds, S Thanoi and S Nudmamud-Thanoi. Regional-specific changes in rat brain BDNF in a model of methamphetamine abuse. *Neuroscience Letters* 2024; **836**, 137880.

[40] S Veerasakul, S Thanoi, GP Reynolds and S Nudmamud-Thanoi. Effect of methamphetamine exposure on expression of calcium binding proteins in rat frontal cortex and hippocampus. *Neurotoxicity Research* 2016; **30(3)**, 427-433.

[41] A Ito, N Usui, M Doi and S Shimada. Adolescent methamphetamine exposure drives neuroinflammation and aberrant neurogenesis linked to anxiety and cognitive impairments in adult mice. *Translational Psychiatry* 2025; **15(1)**, 364.

[42] Y Razavi, F Keyhanfar, A Haghparast, R Shabani and M Mehdizadeh. Cannabidiol promotes neurogenesis in the dentate gyrus during an abstinence period in rats following chronic exposure to methamphetamine. *Metabolic Brain Disease* 2021; **36(6)**, 1381-1390.

[43] H Qiu, M Zhang, C Chen, H Wang and X Yue. Decreasing beta-Catenin leads to altered endothelial morphology, increased barrier permeability and cognitive impairment during chronic methamphetamine exposure. *International Journal of Molecular Sciences* 2025; **26(4)**, 1514.

[44] L Pang and Y Wang. Overview of blood-brain barrier dysfunction in methamphetamine abuse. *Biomedicine & Pharmacotherapy* 2023; **161**, 114478.

[45] H Su, L Zhu, L Su, M Li, R Wang, J Zhu, Y Chen and T Chen. Impact of miR-29c-3p in the nucleus accumbens on methamphetamine-induced

behavioral sensitization and neuroplasticity-related proteins. *International Journal of Molecular Sciences* 2024; **25(2)**, 942.

[46] Y Kusui, N Izuo, R Tokuhara, T Asano and A Nitta. Neuronal activation of nucleus accumbens by local methamphetamine administration induces cognitive impairment through microglial inflammation in mice. *Journal of Pharmacological Sciences* 2024; **154(3)**, 127-138.

[47] S Shi, Y Sun, G Zan and M Zhao. The interaction between central and peripheral immune systems in methamphetamine use disorder: current status and future directions. *Journal of Neuroinflammation* 2025; **22(1)**, 40.

[48] LM Rossi, I Reverte, D Ragozzino, A Badiani, M Venniro and D Caprioli. Role of nucleus accumbens core but not shell in incubation of methamphetamine craving after voluntary abstinence. *Neuropsychopharmacology* 2020; **45(2)**, 256-265.

[49] JR Funke, EK Hwang, AM Wunsch, R Baker, KA Engeln, CH Murray, M Milovanovic, AJ Caccamise and ME Wolf. Persistent neuroadaptations in the nucleus accumbens core accompany incubation of methamphetamine craving in male and female rats. *eNeuro* 2023; **10(3)**, 1-18.

[50] G Lepreux, AM Henricks, G Wei, BS Go, CM Erikson, RM Abella, A Pham and BM Walker. Kappa-opioid receptor antagonism in the nucleus accumbens shell distinguishes escalated alcohol consumption and negative affective-like behavior from physiological withdrawal in alcohol-dependence. *Pharmacology Biochemistry and Behavior* 2024; **243**, 173840.

[51] K Akhoundzadeh and S Shafia. Association between GFAP-positive astrocytes with clinically important parameters including neurological deficits and/or infarct volume in stroke-induced animals. *Brain Research* 2021; **1769**, 147566.

[52] TL Hagemann, S Coyne, A Levin, L Wang, MB Feany and A Messing. STAT3 drives GFAP accumulation and astrocyte pathology in a mouse model of Alexander disease. *Cells* 2023; **12(7)**, 978.

[53] ND Volkow, L Chang, GJ Wang, JS Fowler, D Franceschi, MJ Sedler, SJ Gatley, R Hitzemann, YS Ding, C Wong and J Logan. Higher cortical and lower subcortical metabolism in detoxified methamphetamine abusers. *American Journal of Psychiatry* 2001; **158(3)**, 383-389.

[54] DR Miller, M Bu, A Gopinath, LR Martinez and H Khoshbouei. Methamphetamine dysregulation of the central nervous system and peripheral immunity. *Journal of Pharmacology and Experimental Therapeutics* 2021; **379(3)**, 372-385.

[55] R Kuczenski, IP Everall, L Crews, A Adame, I Grant and E Masliah. Escalating dose-multiple binge methamphetamine exposure results in degeneration of the neocortex and limbic system in the rat. *Experimental Neurology* 2007; **207(1)**, 42-51.

[56] M Pekny and M Pekna. Astrocyte reactivity and reactive astrogliosis: Costs and benefits. *Physiological Reviews* 2014; **94(4)**, 1077-1098.

[57] F Leipp, J Vialaret, P Mohaupt, S Coppens, A Jaffuel, AC Niehoff, S Lehmann and C Hirtz. Glial fibrillary acidic protein in Alzheimer's disease: A narrative review. *Brain Communications* 2024; **6(6)**, fcae396.

[58] JE Burda and MV Sofroniew. Reactive gliosis and the multicellular response to CNS damage and disease. *Neuron* 2014; **81(2)**, 229-248.

[59] S Tolomeo and R Yu. Brain network dysfunctions in addiction: A meta-analysis of resting-state functional connectivity. *Translational Psychiatry* 2022; **12(1)**, 41.

[60] X Wen, L Yue, Z Du, L Li, Y Zhu, D Yu and K Yuan. Implications of neuroimaging findings in addiction. *Psychoradiology* 2023; **3**, kkad006.

[61] A Sivils, JQ Wang and XP Chu. Striatonigrostriatal spirals in addiction. *Frontiers in Neural Circuits* 2021; **15**, 803501.

[62] SN Haber, JL Fudge and NR McFarland. Striatonigrostriatal pathways in primates form an ascending spiral from the shell to the dorsolateral striatum. *The Journal of Neuroscience* 2000; **20(6)**, 2369-2382.

[63] LH Corbit, H Nie and PH Janak. Habitual alcohol seeking: Time course and the contribution of subregions of the dorsal striatum. *Biological Psychiatry* 2012; **72(5)**, 389-395.

[64] FS Alshehri, YS Althobaiti and Y Sari. Effects of administered ethanol and methamphetamine on glial glutamate transporters in rat striatum and hippocampus. *Journal of Molecular Neuroscience* 2017; **61(3)**, 343-350.

[65] A Zahra, O Samareh, N Somayeh, VN Saeed, RA Navid, A Mohammad-Amin, T Foozhan, M Gholam-Reza, A Hojjat Allah and D Shahram. Exploring amygdala structural changes and signaling pathways in postmortem brains: Consequences of long-term methamphetamine addiction. *Anatomy & Cell Biology* 2024; **57(1)**, 70-84.

[66] S Jayanthi, AP Daiwile and JL Cadet. Neurotoxicity of methamphetamine: Main effects and mechanisms. *Experimental Neurology* 2021; **344**, 113795.

[67] X Chen, F Qiu, X Zhao, J Lu, X Tan, J Xu, C Chen, F Zhang, C Liu, D Qiao and H Wang. Astrocyte-derived lipocalin-2 is involved in mitochondrion-related neuronal apoptosis induced by methamphetamine. *ACS Chemical Neuroscience* 2020; **11(8)**, 1102-1116.

[68] T Canedo, CC Portugal, R Socodato, TO Almeida, AF Terceiro, J Bravo, AI Silva, JD Magalhaes, S Guerra-Gomes, JF Oliveira, N Sousa, A Magalhaes, JB Relvas and T Summavielle. Astrocyte-derived TNF and glutamate critically modulate microglia activation by methamphetamine. *Neuropsychopharmacology* 2021; **46(13)**, 2358-2370.

[69] AS Gibson, PJ West and KA Keefe. Effects of methamphetamine-induced neurotoxicity on striatal long-term potentiation. *Psychopharmacology* 2022; **239(1)**, 93-104.

[70] J Ding, J Huang, X Tang, L Shen, S Hu, J He, T Liu, Z Yu, Y Liu, Q Wang, J Wang, N Zhao, X Qi and J Huang. Low and high dose methamphetamine differentially regulate synaptic structural plasticity in cortex and hippocampus. *Frontiers in Cellular Neuroscience* 2022; **16**, 1003617.

[71] M Gonzalez-Rodriguez, S Villar-Conde, V Astillero-Lopez, P Villanueva-Anguita, I Ubeda-Banon, A Flores-Cuadrado, A Martinez-Marcos and D Saiz-Sanchez. Neurodegeneration and astrogliosis in the human CA1 hippocampal subfield are related to hsp90ab1 and bag3 in Alzheimer's disease. *International Journal of Molecular Sciences* 2021; **23(1)**, 165.

[72] LA Welikovitch, A Mate de Gerando, A Khasnavis, H Bhavsar, JC Meltzer, L Buee, LB Chibnik, T Bussiere and BT Hyman. Tau, synapse loss and gliosis progress in an Alzheimer's mouse model after amyloid-beta immunotherapy. *Brain* 2025; **148(4)**, 1316-1328.

[73] P Shi, Z Li, T He, N Li, X Xu, P Yu, X Lu, J Nie, D Liu, Q Cai, Y Guan, F Ge, J Wang and X Guan. Astrocyte-selective STAT3 knockdown rescues methamphetamine withdrawal-disrupted spatial memory in mice via restoring the astrocytic capacity of glutamate clearance in dCA1. *Glia* 2021; **69(10)**, 2404-2418.

[74] Y Schneider, C Gauer, M Andert, A Hoffmann, MJ Riemenschneider, W Krebs, N Chalmers, C Lötzsch, UJ Naumann, W Xiang, V Rothhammer, R Beckervordersandforth, JCM Schlachetzki and J Winkler. Distinct forebrain regions define a dichotomous astrocytic profile in multiple system atrophy. *Acta Neuropathologica Communications* 2024; **12(1)**, 1.

[75] T Samikkannu, KVK Rao, AAA Salam, VSR Atluri, EM Kaftanovskaya, M Agudelo, S Perez, C Yoo, AD Raymond, H Ding and MPN Nair. HIV subtypes B and C gp120 and methamphetamine interaction: Dopaminergic system implicates differential neuronal toxicity. *Scientific Reports* 2015; **5**, 11130